Dispersion of Single-Walled Carbon Nanotubes in Poly(ϵ-caprolactone)

Cynthia A. Mitchell and Ramanan Krishnamoorti*

Department of Chemical and Biomolecular Engineering, University of Houston, Houston, Texas 77204-4004

Received July 17, 2006; Revised Manuscript Received November 17, 2006

ABSTRACT: The dispersion of single-walled carbon nanotubes (SWNT) in poly(ϵ-caprolactone) with the aid of a zwitterionic surfactant is reported. Melt rheology and electrical conductivity measurements indicate geometrical percolation and electrical percolation for nanocomposites with ∼0.08 wt % SWNT, implying an effective anisotropy for the nanotubes of at least 600. Spectroscopic measurements and comparison of dispersion using other surfactants established that the excellent dispersion is a result of the compatibilizing effect of the zwitterionic surfactant.

Introduction

Single-walled carbon nanotube (SWNT)-based polymer nanocomposites have the potential for tailoring of unique lightweight materials with enhanced mechanical, thermal, and electronic properties.[1] A major technological impediment for the development of such nanocomposites and realization of the extraordinary combinations of properties stems from the lack of dispersability of the SWNTs with the as-produced SWNTs being held together in ropes or bundles of ropes by van der Waals forces. Several approaches have been implemented, including covalent functionalization of nanotubes,[2] dispersion of individual nanotubes in a polymerizable monomer,[3] and surfactant-assisted dispersions.[4,5] In this paper we report the effective dispersion of pristine nonfunctionalized SWNTs in poly(ϵ-caprolactone) using a compatibilizing zwitterionic surfactant.

The choice of the polymer, poly(ϵ-caprolactone) (PCL), was largely dictated by previous reports that the monomer (ϵ-caprolactone) can effectively disperse laser ablation produced SWNTs;[6] thus, compatibility between the SWNT and the PCL was anticipated. In fact, the dispersion of the high-pressure carbon monoxide (HiPco) process produced SWNTs in ϵ-caprolactone is quite good as evidenced by the sharp van Hove absorption bands for these dispersions (Figure 1). In particular, we note that no surfactants or other compatibilizing agents were used in the preparation of this dispersion.

Solvent assisted or melt mixtures of PCL and pristine SWNTs result in poorly dispersed systems and suggest that for thermodynamic or kinetic reasons the favorable interactions between the monomer and the nanotubes do not result in the formation of well-dispersed polymer nanocomposites. Surfactants have been utilized successfully to aid in the dispersion of individual SWNTs or smaller bundles of SWNTs in aqueous solution[7,8] and in composites.[5,9] Amines have been shown to favorably interact with SWNTs,[10,11] and stable dispersions of SWNTs with octyldecylamine in THF have been observed.[12,13] Two mechanisms for the amine surfactant-assisted dispersion of the nanotubes have been proposed. One is by which a zwitterion is formed with the carboxyl functionalities observed on SWNT ends or from sidewall defects.[13,14] The second mechanism for dispersion has been attributed to the physisorption of the amines along the sidewalls of the nanotubes. In both cases, and noting a recent study by Matarredona et al.[15] where they observed that the minimum amount of surfactant needed to disperse the SWNTs was well below the critical micelle concentration (cmc) of the surfactant since the effective dispersion was found to be due to adsorbed surfactant and not to the solubilization of the SWNTs in the interior of a cylindrical micelle,[8] it is reasonable to assume that at least in the case of amine-based surfactants a small amount of surfactant can result in an effective dispersion. In this work we use a small amount of a zwitterionic surfactant to establish compatibility between PCL and SWNTs.

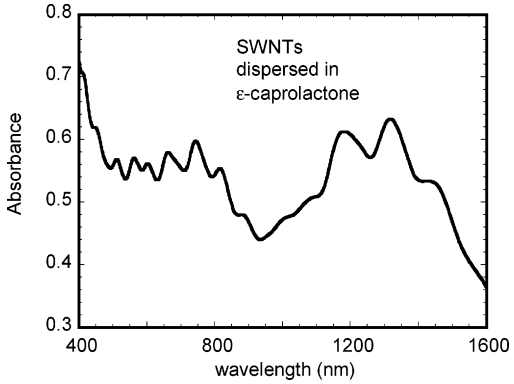

Figure 1. Absorption spectra for SWNTs (HiPco) dispersed in ϵ-caprolactone by sonication and subsequent centrifugation. Dispersion and the presence of individualized or small bundles of tubes are established by the characteristic van Hove singularities observed between 400 and 1500 nm. The absorption spectra shown here are considerably sharper than those obtained with laser ablation nanotubes as shown by Ausman et al.[6]

While it is challenging to probe the state of dispersion of SWNTs in polymers because of the high aspect ratio of the tubes and their relatively poor electron density contrast with hydrocarbon-based polymers, we have resorted to several different probes that interrogate the structure at different length scales and can hence provide overall information regarding the state of dispersion. Local probes such as absorption spectroscopy (with the characteristic sharp van Hove singularities for dispersed nanotubes) and electron microscopy are used in conjunction with small-angle X-ray scattering, an intermediate length scale probe, and mesoscale probes exploiting melt rheology and electrical conductivity.

Experimental Section

The polymer used in this study was poly(ϵ-caprolactone) (PCL) (Aldrich Chemical Co.) and was used as received. The weight-average molecular weight, M_w, was 65 000 Da, and the number-

10.1021/ma0616054 CCC: $37.00
Published on Web 02/03/2007

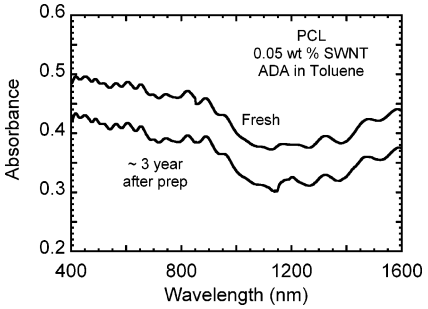

Figure 2. Absorption spectra for the toluene solution containing 0.05 wt % SWNT dispersed with ADA and stabilized by the addition of PCL right after preparation (Fresh) and ~3 years later. The data are shifted vertically for clarity. The van Hove singularities and other spectral features are quite similar for the two spectra and indicate no tendency of the nanotubes to reaggregate in the toluene solution.

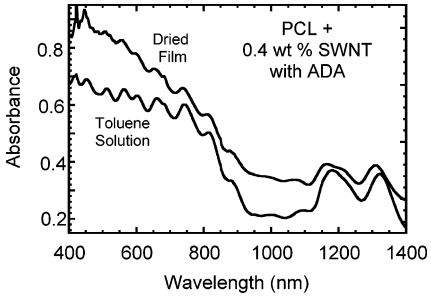

Figure 3. Absorption spectra for the PCL nanocomposite containing 0.4 wt % SWNT dispersed with ADA in toluene (as-prepared with no centrifugation) and the corresponding thin film nanocomposite. Dispersion and the presence of individualized or small bundles of tubes are established by the characteristic van Hove singularities observed between 400 and 1400 nm.

average molecular weight, M_n, was 42 500 Da. The SWNTs used were produced by the HiPco process[16] (from Carbon Nanotechnologies Inc.) and purified according to literature methods.[10] The nanotubes were dispersed in toluene (~10 mg in 50 mL of solvent) with the aid of 12-aminododecanoic acid (ADA) (Aldrich Chemical Co., used as received), a zwitterionic surfactant, and assisted by sonication. Sonication was performed using a Fisher Scientific ultrasonic bath cleaner with an output frequency of 44 kHz for ~3 h. The ratio of amine head group to nanotube carbon (molar ratio) was maintained at 1:70 for the majority of this study, and variations in the surfactant loading are noted when deviated from this amount. The polymer was added to this suspension in toluene after sonication. We note that the nanotube dispersion in toluene, without centrifugation to remove bundles or aggregates, appears to be significantly stabilized by the addition of the polymer; i.e., there is much less propensity for nanotubes to settle out in the presence of the polymer. While it is tempting to argue that this is a kinetic phenomenon based on the increased solution viscosity, we report unchanged dispersion states after over 3 years of letting the sample to attain equilibrium under quiescent conditions (Figure 2). To prepare the polymer hybrids, the solvent was removed by extensive drying under ambient conditions followed by vacuum drying at room temperature with subsequent vacuum drying in the melt state (100 °C) for at least 24 h.

UV−vis−near-IR measurements were performed using a Jasco V570 spectrophotometer over a wavelength range of 400−1600 nm. Solution spectra were obtained using a 1 mm path length quartz cuvette, and the nanocomposite films were melt-pressed to a thickness of 140 μm and the spectra obtained on free-standing films. FTIR spectra were recorded on a ThermoNicolet 4700 FTIR. 72 scans per sample were collected with a resolution of 4 cm^{-1}. Samples for FTIR were prepared by solution-casting dilute solutions onto NaCl windows and evaporating the solvent in a vacuum oven at 50 °C. For scanning electron microscopy (SEM), bulk samples were sputtered with gold to prevent charging, and the surface morphology of the SWNT-based PCL nanocomposites was probed using a Philips scanning electron microscope (SEM) at an accelerating voltage of 30 kV.

Samples for melt rheology were prepared by vacuum-molding ~1 g of the sample in a 25 mm die and pressing in a Carver press at 80 °C for 1 h using a maximum 1 ton load. Melt-state rheological measurements were performed on a TA Instruments ARES rheometer with a torque transducer range of 0.2−2000 g_f cm using 25 mm diameter parallel plates with a sample thickness of 1−2 mm and a temperature range of 65−90 °C. An oscillatory strain ($\gamma(t)$) of the form

$$\gamma(t) = \gamma_0 \sin(\omega t) \tag{1}$$

is applied where γ_0 is the strain amplitude (always less than 0.15 in the studies reported here and typically below 0.02) and ω is the frequency. The resulting time-dependent linear shear stress ($\sigma(t)$) is interpreted as

$$\sigma(t) = \gamma_0(G' \sin(\omega t) + G'' \cos(\omega t)) \tag{2}$$

where G' and G'' are the storage and loss modulus, respectively. All measurements in this study were verified to be linear (i.e., G' and G'' independent of γ_0) and interpreted using eq 2. Additional rheological parameters used in this study include the complex modulus G^* ($= \sqrt{(G')^2+(G'')^2}$) and the complex viscosity η^* ($= G^*/\omega$).

Electrical conductivity characterization of the nanocomposites was performed using measurements of dc resistance utilizing a two-point probe at room temperature. The dc conductivity (σ_{dc}) was obtained from

$$\sigma_{dc} = \frac{t}{RA} \tag{3}$$

where R is the dc resistance, t is the thickness of the sample, and A is the sample cross-sectional area. Samples were typically 0.5−1 mm thick and ~1 cm^2 in cross-sectional area and prepared by vacuum molding.

Small-angle X-ray scattering (SAXS) measurements were performed at the National Synchrotron Light Source (NSLS) at Brookhaven National Laboratory Beamline X27C with a wavelength (λ) of 1.371 Å with a beam diameter of ~0.5 mm at the sample. Samples were prepared as discs of 7 mm diameter and 1.5 mm thick and placed in brass annular holder with Kapton tape windows and heated in a dual chamber oven with the measurements reported in the paper being performed in the melt state of the polymer at 80 °C. The collected data were corrected for background scattering and empty cell scattering using standard methods.[11]

Results and Discussion

The UV−vis−near-IR absorption spectra from an as-prepared solution of SWNTs dispersed in toluene with the aid of 12-aminododecanoic acid (ADA) and to which the polymer was added (0.4 wt % SWNT with respect to the total polymer amount and not related in any way to the amount of solvent used) and that from a dried film of the same nanocomposite are shown in Figure 3. UV−vis−near-IR spectroscopy provides a good indication of the dispersion quality of SWNTs in solvents,[17] surfactant-assisted solutions of SWNTs,[7] and SWNT-based polymer composites.[9] Smaller bundles and individually dispersed nanotubes exhibit pronounced van Hove singularities while larger bundles of SWNTs and their aggregates exhibit broadened or less sharp features or display no distinctive features other than a monotonically decreasing absorption with increasing wavelength.[1,13] The characteristic peaks associated with the van Hove transitions are observed in the spectra of the solution

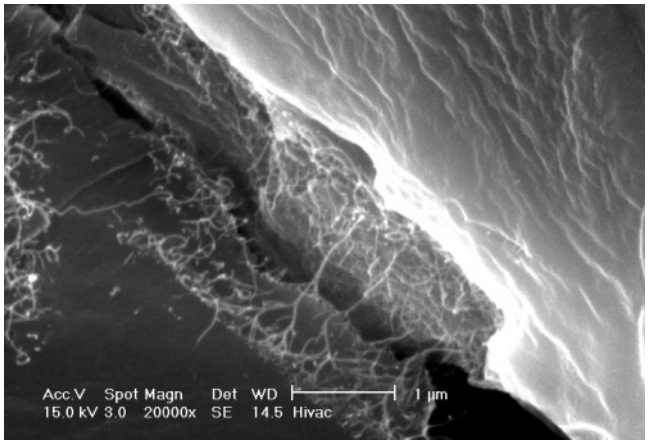

Figure 4. Scanning electron micrograph (SEM) of a fracture surface following tensile testing of a 0.1 wt % SWNT-based PCL nanocomposite. The image is representative of the fracture surface observed for samples with nanotube loadings ranging from 0.05 to 0.4 wt %.

(Figure 3) at all concentrations of the nanotubes. For the nanocomposite film, no significant broadening of the van Hove transitions is observed. Also, the absorption peaks for the nanocomposite are at the same positions as in the solution in toluene.

The zwitterionic surfactant helps disperse the SWNTs as individuals or as small bundles presumably by favorable interactions between the amine headgroup and the nanotubes. It has been shown previously through small-angle neutron scattering and other analytical techniques that a very small fraction of the surfactant molecules participate in the solubilization of the SWNTs even in water.[6,13,15] Upon addition of PCL, the dispersion is maintained by the development of favorable hydrogen-bonding interactions between the surfactant and PCL (as demonstrated later) and resulting in compatibilization between the nanotubes and the polymer. This, in conjunction with the inherent compatibility between ϵ-caprolactone and SWNTs (Figure 1),[6] results in well-dispersed nanotubes in PCL.

The state of dispersion is further corroborated by SEM which exhibited no large-scale aggregates, and well-dispersed nanotubes are observed (Figure 4). Optical and atomic force micrographs at room temperature could not be used to conclusively ascertain the state of dispersion due to the crystallization of the PCL and are in fact excellent probes for the crystalline structure of the PCL. Nevertheless, both those structural studies indicated the absence of large aggregates in the samples.

Several studies have utilized X-ray and neutron based small-angle scattering to probe the structure of SWNTs[8,18] and other nanoparticles in solution[19] and in composites,[20] and we follow those protocols in this work. Figure 5 shows small-angle X-ray scattering (SAXS) data in the *melt state* for the series of nanocomposites. The data in Figure 5a demonstrate that the q dependence of the scattered intensity is featureless and monotonically decreasing with increasing q. The q dependence of the scattered intensity, particularly at low q, is better observed in Figure 5b where the product of Iq^2 is plotted. From these data it is clear that for q values from 0.01 to 0.04 Å^{-1} the SANS intensity scales as q^{-2}. In light of the estimated R_g of the PCL of ~70 Å[21] and the expected q^{-1} scaling associated with individualized SWNTs, the q^{-2} scaling is surprising. The origins of the q^{-2} dependence could arise from an altered conformation of the PCL chains in the melt, or from aggregates or fractal-like structure of nanotubes, or from the intrinsic coil-like conformation and hence q^{-2} form factor based scattering of the SWNTs or SWNT ropes.[22]

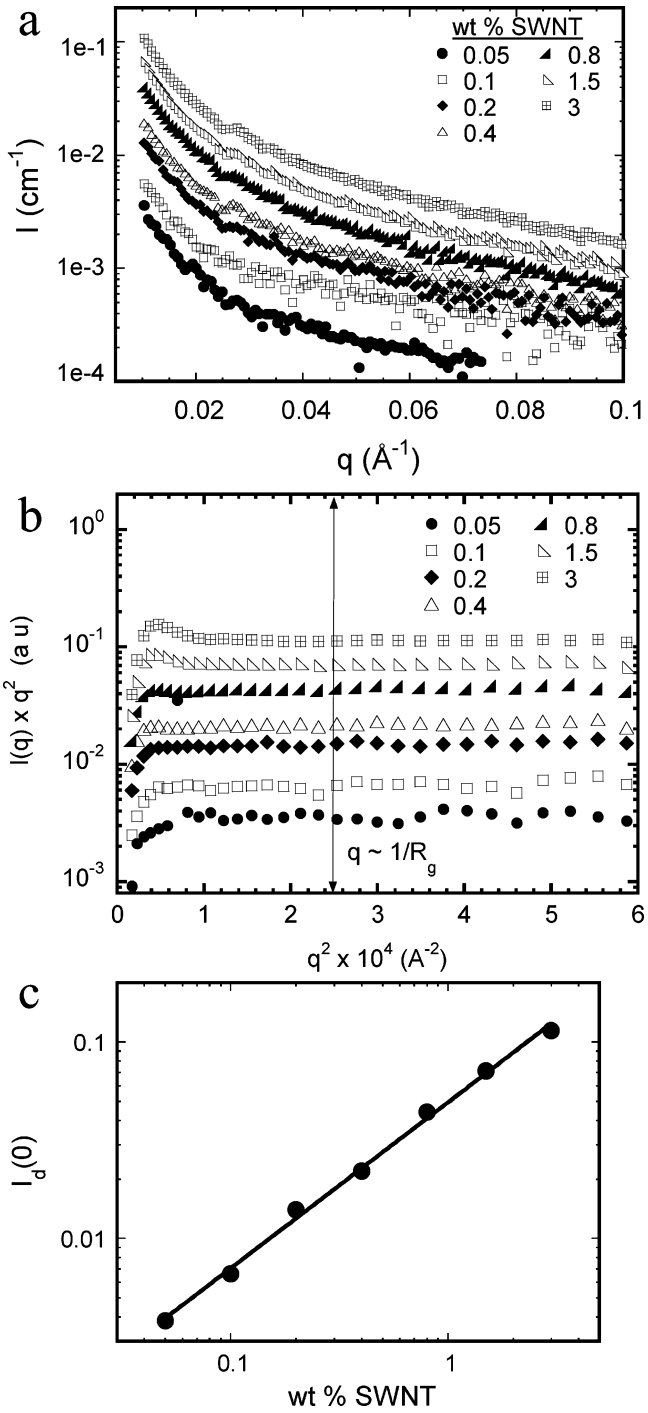

Figure 5. Small-angle X-ray scattering (SAXS) data in the melt state for the series of PCL nanocomposites ($T = 80$ °C). The dependence of $I(q)$ with q is featureless and monotonically decreases with increasing q for each sample. The q dependence is much better observed in a plot of the product of Iq^2 vs q. This demonstrates that the low-q intensity for all the nanocomposites exhibit q^{-2} dependence. The similarity of the q scaling of the intensity for all the nanocomposites (0.05−3 wt %) along with the presence of qualitatively similar UV−vis−near-IR spectra suggests that the state of aggregation of the tubes does not change with increasing PCL concentration. The average value of the plateau value of the product of $I(q)q^2$ (denoted as $I_d(0)$) for the different nanocomposites is plotted in part c and demonstrates a power-law dependence with SWNT concentration (scaling as $\phi_{SWNT}^{0.8}$).

Of these, the altered conformation of PCL chains is perhaps the easiest to rule out. The inclusion of only 0.05 wt % SWNT appears to have altered the conformations of all of the chains, and any further addition of SWNTs has virtually no effect on the conformations of the polymer. Further, the persistence of

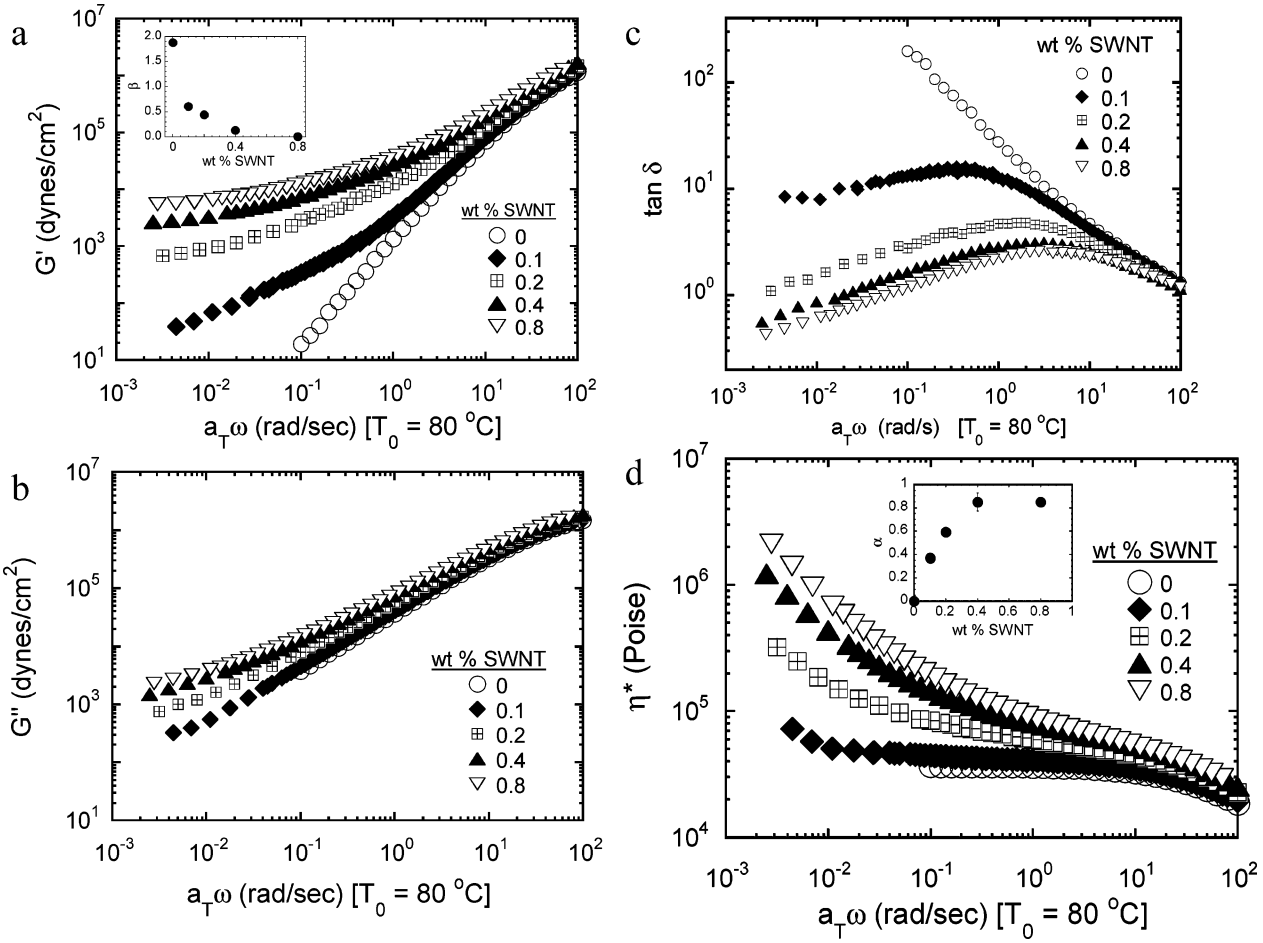

Figure 6. Master curves for the frequency dependence of the storage modulus G' (a), loss modulus G'' (b), loss tangent tan δ (c), and complex viscosity η^* (d) for the pure polymer and the nanocomposites (all compatibilized using ADA). The nanocomposites with a loading of 0.1 wt % SWNT demonstrate solidlike characteristics at low frequencies with the presence of a plateau or frequency independence in G'. The insets of (a) and (d) demonstrate the low-frequency power law exponents of G' and η^* (β and α, respectively) obtained by power-law fitting of G' and η^* for the five lowest frequencies.

the q scaling from 0.05 up to 3 wt % and with no crossover to a stronger q dependence at high concentrations of nanotubes, as would be expected from non-self-similar larger ropes or aggregates, along with the previously demonstrated optical spectra to demonstrate the presence of individualized nanotubes suggest that the observed q scaling is not from non-self-similar aggregate structure of the nanotubes. Additionally, the value of the product Iq^2 at low q values scales as $(\phi_{SWNT})^{0.8}$, as shown in Figure 5(c). This scaling is similar to the intensity scaling for a Gaussian polymer chain in a good solvent[23] and suggestive of the fact that the nanotubes or small diameter ropes of SWNT are well-dispersed in a good solvent of the PCL chains. Alternatively, the nanotubes adopt a self-similar fractal-like structure and these structures dominate the observed scattering. Further, this would also require that the internal scaling of the fractal dimensions remains unchanged over a concentration of nanotubes ranging from 0.05 to 3 wt %.

Previously, melt-state rheology has been shown to be a powerful probe of the mesoscale dispersion of nanoparticles, including highly anisotropic layered silicates, functionalized SWNTs, and MWNTs.[5,24,25] Only the smallest possible oscillatory strain amplitudes were employed so as to obtain a linear stress response and apply minimal deformation on the microstructure and not alter the quiescent state structure of the nanocomposite. The melt rheology data were superposed using the Boltzmann principle of time−temperature superpositioning to obtain master curves. Horizontal (frequency) shift factors (a_T) were applied, and no vertical (modulus shifts) were necessary. The shift factors for the nanocomposites are similar to those of the unfilled polymer and obey an Arrhenius-type temperature dependence with an activation energy of ~19 kJ/mol.[21]

The viscoelastic functions storage modulus G', loss modulus G'', loss tangent (tan δ), and complex viscosity η^* for the pure polymer and the nanocomposites are shown in Figure 6. The pure polymer behaves as a Newtonian liquid at low frequencies with $G' \propto \omega^2$, $G'' \propto \omega^1$, and $\eta^* \propto \omega^0$. We note that the crossover frequency (i.e., frequency at which G' and G'' intersect) and the plateau region for the polymer relaxation are not accessible in the current measurements. The low-frequency response for the nanocomposites, on the other hand, display an increase in the value of G', a decrease in the frequency dependence of G' (i.e., $G' \propto \omega^\beta$, with $\beta < 2$), an increase in the value of η^*, and an increased frequency dependence (i.e., low-frequency divergence) of η^* (i.e., $\eta^* \propto \omega^{-\alpha}$, with $0 < \alpha < 1$) and indicates solidlike character for them. In the insets of parts a and d of Figure 6, the exponents β and α, respectively (obtained by fitting of five lowest frequency data points), are plotted as a function of nanotube concentration. The values of α increase monotonically from 0 to 0.8, and the value of β decreases monotonically from 2 to 0.2 with increasing nanotube concentration. While these viscoelastic property changes for these nanocomposites are similar to those of soft glassy materials,[26] the loss tangent data clearly indicate that the viscoelastic properties, even at low frequencies, do not superpose to form time−temperature−

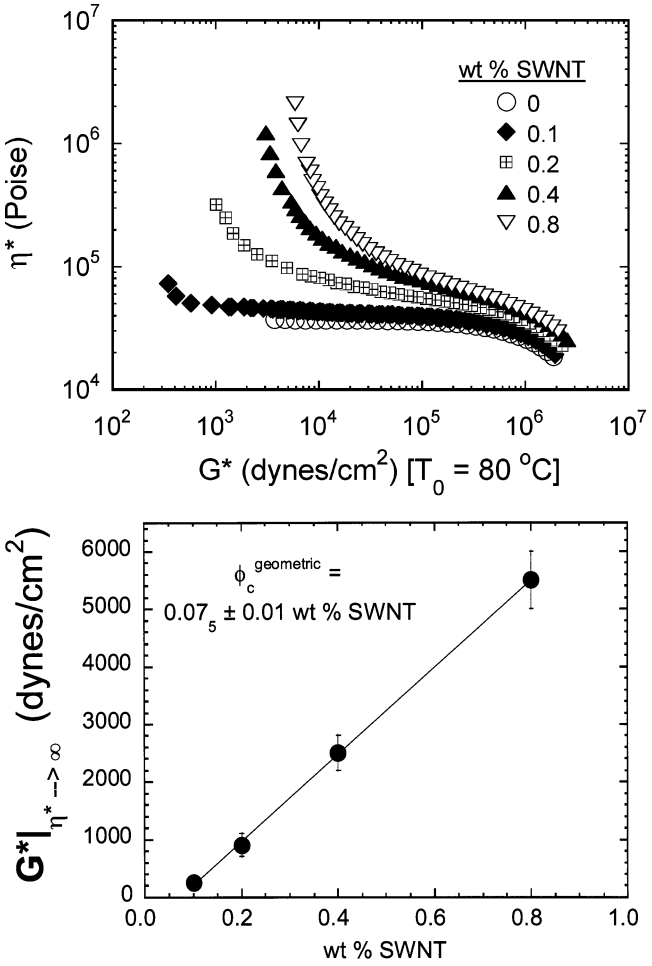

Figure 7. Accompanying the formation of a percolated filler structure is the development of a finite yield stress which is demonstrated by a divergence in a cross plot of the complex viscosity (η^*) vs the complex modulus (G^*) for all the nanocomposites, while the pure polymer exhibits Newtonian behavior. The line shown in the bottom figure represents a linear fit of $G^*|_{\eta^*\to\infty}$ with nanotube loading to extract the percolation threshold denoted as $\phi_c^{\text{geometric}}$.

composition master curves[27] and indicate that the polymer affects the solidlike nature of these nanocomposites that presumably arises from a percolation of the nanotubes.

The formation of such nanotube (or nanoparticle) network structure that leads to an elastic reinforcement and the transformation of liquidlike polymer response to solidlike response have been documented previously for SWNTs,[2,5] MWNTs,[4] layered silicates,[28] silica nanoparticles,[25] and carbon black.[29] Associated with the formation of a percolated network structure is the development of a finite yield stress[30] which is manifested as a diverging η^* at a finite value of G^*, as shown in Figure 7 and resulting in a percolation threshold of 0.07_5 wt % SWNT by linear extrapolation of the value of $G^*|_{\eta^*\to\infty}$ to zero. This divergence has been correlated with steady shear measurements at low shear rates and creep measurements in previously studied layered silicate nanocomposites to a measured finite yield stress and confirms in this case the development of solidlike behavior at a nanotube loading as low as 0.1 wt %.[31] The hydrodynamic manifestation of geometrical percolation threshold is dependent upon the largest dimension (ℓ) and the effective anisotropy (ℓ/d) of the nanoparticle or aggregate of nanoparticles that cannot be further separated. Calculations for the percolation of ellipsoids (with no excluded volume),[32] for a system where geometrical percolation of the primary objects occurs $\sim 7._5 \times 10^{-4}$ vol % ($= 0.07_5$ wt % SWNT), indicate that the effective

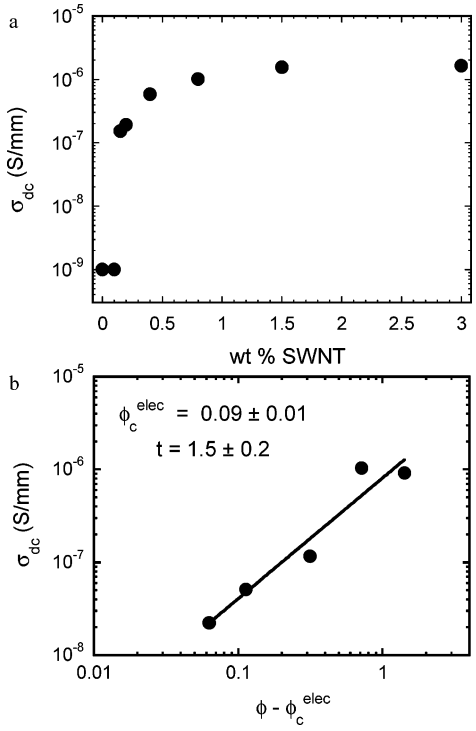

Figure 8. Composition dependence of the dc conductivity obtained from a two-point probe (a). The conductivity for the pure polymer (and the polymer with added ADA and not shown) is below the lower threshold of the instruments and is merely reported as 10^{-9} S/mm The percolation threshold (ϕ_c^{elec}) is easily obtained by a best fit to a plot of σ_{dc} vs ($\phi - \phi_c^{\text{elec}}$) (b).

geometric anisotropy or ℓ/d is $\sim$700 or more. These results indicate that the nanotubes are indeed well dispersed in the PCL matrix.

We investigated the solid-state electrical conductivity by dc conductivity measurements as a function of SWNT concentration to examine whether the geometrical percolation noted in the melt-state rheological experiments has consequences on the solid-state (i.e., crystalline state of the polymer) electrical properties of the nanocomposites.[33] Figure 8a shows a plot of the dc conductivity as a function of SWNT concentration. The volume resistance of the pure polymer and the mixtures of polymer and surfactant were beyond the limits of the two-point probe used ($<10^{-9}$ S/mm). The measured conductivity as a function of nanotube concentration to a first approximation follows

$$\sigma_{\text{dc}} = C(\phi - \phi_c^{\text{elec}})^t \tag{4}$$

where σ_{dc} is the dc conductivity, ϕ_c^{elec} is the concentration of nanotubes at the electrical percolation, t is a universal scaling exponent, and C is a constant.[34] The data near the percolation threshold fit eq 4 well and suggest good agreement with the underlying theory. From Figure 8b a percolation threshold weight fraction $\phi_c^{\text{elec}} = 0.09 \pm 0.01$ and a scaling exponent $t = 1.5 \pm 0.2$ were extracted. The value of t lies between those expected for charge transport in two dimensions ($t = 1.33$) and three dimensions ($t = 2$). However, we note that the value of t is similar to those observed in many other bulk composites and nanocomposites. The proximity of the experimentally determined exponent to the two-dimensional transport exponent is thought to originate from thermally induced hopping between loosely connected elements of a percolative network.

Such a low value for the electrical percolation threshold is consistent with the geometrical percolation obtained by melt

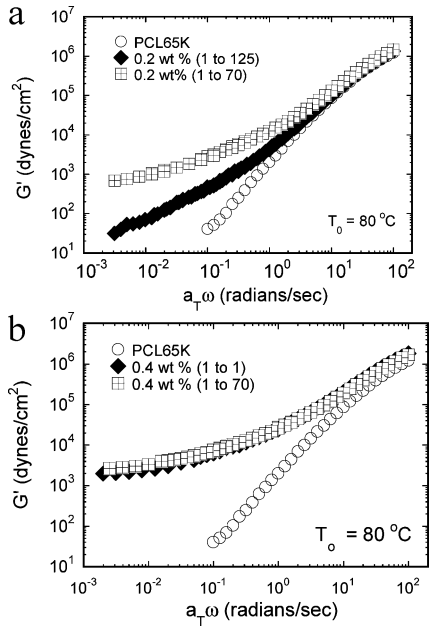

Figure 9. Comparison of the storage modulus, G', for the nanocomposites prepared using different ratios of ADA molecules to number of SWNT carbons. A ratio of 1:125 does not lead to an adequate dispersion (a) while a ratio of 1:1 (b) yields no significant improvement in dispersion.

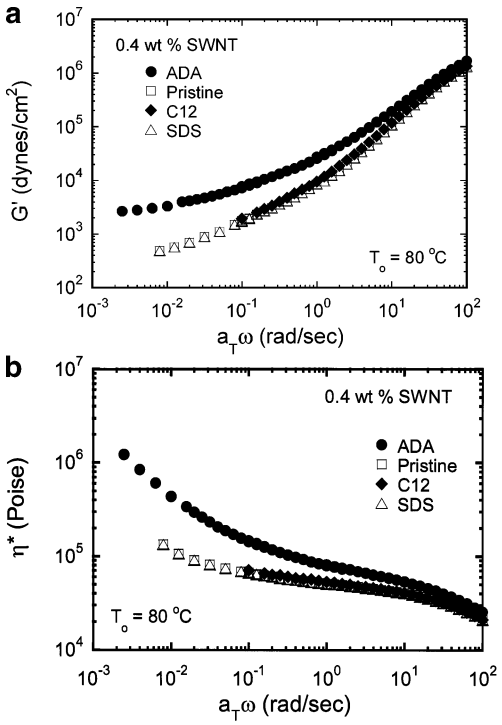

Figure 10. Comparison of the storage modulus, G' (a), and the complex viscosity, η^* (b), for the nanocomposites prepared utilizing different surfactants. The nanocomposite prepared with ADA exhibits marked improvement in dispersion over that of the nanocomposites prepared with pristine SWNTs and those prepared with C12 and SDS. The surfactant molecule to SWNT carbon ratio was 1:70 for all of the surfactant assisted nanocomposites.

rheology and comparable to SWNTs in epoxy (0.1−0.2 wt %)[35] and SWNTs in PEO (0.03 wt %).[5] The electrical percolation threshold is dependent upon a number of factors such as particle shape, particle−particle interactions, the dispersion state of the conducting fillers in the polymeric matrix, and processing conditions. Nevertheless, the low value for ϕ_c^{elec} confirms the

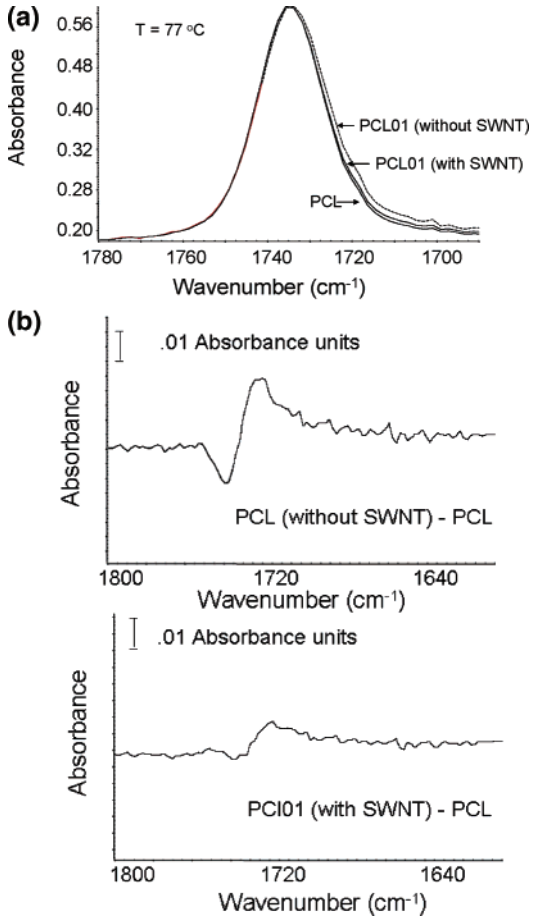

Figure 11. (a) FTIR spectra in the carbonyl stretching region for PCL and the ADA assisted SWNT nanocomposite with a loading of 0.1 wt %. For comparison, a sample containing the same amount of ADA but without SWNT is included. A broadening of the carbonyl peak at low wavenumbers is indicative of hydrogen bonding. (b) Difference FTIR spectra demonstrating the changes in the carbonyl stretching region for the PCL-based nanocomposites.

previous observations indicating excellent dispersion of the SWNTs in PCL.

While no systematic attempt was made to optimize the ratio of surfactant to SWNT needed to achieve the best dispersion, a preliminary study of surfactant to nanotube ratios indicated that the studies carried out here with 1:70 ratio of ADA molecules per SWNT carbon led to dispersions that were largely independent of the specific surfactant to nanotube ratio. Three different ratios of ADA to SWNT were examined (1:70, 1:125, and 1:1 ADA molecules per SWNT carbon atom) and studied. As shown in Figure 9, the 1:125 loading does not lead to adequate dispersion of the SWNTs. On the other hand, no substantial differences in rheological properties are observed for the 1:70 and 1:1 nanocomposites and indicate that additional amounts of surfactant beyond the 1:70 ratio does not lead to any significant improvement in the dispersion of the nanotubes.

We addressed the mechanism for dispersion of the SWNTs in PCL assisted by the zwitterionic surfactant ADA using two different strategies. First, we examined at comparable loadings the influence of altering the surfactant and specifically the head group. In particular, we present the rheological data for SWNT nanocomposites with dodecyltrimethylammonium bromide (C12), sodium dodecyl sulfonate (SDS), and ADA and compare that to a mixture of PCL with pristine uncompatibilized SWNTs in Figure 10. In all cases the amount of surfactant added was maintained at 1 surfactant molecule for every 70 SWNT carbon

atoms. Of these surfactants, there have been several reports in the literature that indicate that SDS disperses the SWNTs in water.[8,15,36] Clearly, in the case of the ADA compatibilized SWNTs there is marked increase in the low-frequency modulus values and therefore improvement in the dispersion state of the nanotubes, and the other two surfactant compatibilized systems were comparable to the dispersion of pristine SWNTs in PCL. Thus, we conclude that in comparison to the other surfactants, in the presence of poly(ϵ-caprolactone), the zwitterionic surfactant ADA has better interactions with the nanotubes, resulting in better dispersions.

We further examined the nature of interactions between the nanotubes, polymer, and the surfactant (ADA) using FTIR measurements. Measurements were performed in the melt state to avoid any complications from the differences in crystalline structure of the polymer. We focus our attention here on the carbonyl stretch of the PCL, which is most sensitive to intermolecular interactions. The amide bands (3300−3600) of the surfactant were examined with much thicker samples because of the low concentration of the surfactant in the nanocomposites and demonstrated no differences between the samples of PCL and ADA with and without SWNTs. The carbonyl group of PCL is known to develop strong intermolecular hydrogen bonds with various polymers[37] which contain hydroxyl groups as well as several low-molecular-weight amino compounds.[38] Figure 11 shows the FTIR spectra in the carbonyl stretching region for PCL and the ADA assisted SWNT nanocomposite. For comparison, a sample containing the same amount of ADA in PCL without SWNT was prepared. For the ADA prepared samples with and without SWNT there is a broadening of the carbonyl peak on the low wavenumber side associated with the vibration of the hydrogen-bonded carbonyls. These are more clearly observed in the difference spectra presented that clearly show the increase in the low wavenumber peak and a diminishing of the high wavenumber peak for the nanocomposites as compared to the pure polymer. We note that the addition of SWNTs to a mixture of PCL and ADA results in the sacrifice of some of the favorable interactions between PCL and ADA to enable favorable interactions between the SWNT and ADA and thereby compatibilize the PCL and SWNTs. From the FTIR measurements we conclude that the zwitterionic ADA surfactant results in interactions with the poly(ϵ-caprolactone) through strong chemical interactions. Further combining with the ability of ADA to disperse nanotubes in solvents such as toluene, we conclude that ADA acts as a compatibilizer that interacts with both the nanotubes and the polymer.

Concluding Remarks

We have shown using a range of characterization techniques that SWNTs can be effectively dispersed (with effective aspect ratios of ~600 or greater) in a polyester matrix using a surfactant capable of interacting with both the SWNTs and the polymer. Such an excellent dispersion is achieved by the compatibilizing effect rendered by the zwitterionic surfactant that has favorable interactions with both the SWNTs and the polymer. The consequences of such an excellent dispersion of the nanotubes on the thermomechanical properties of the nanocomposites such as the crystallization morphologies, crystallization kinetics, glass transition, linear elastic modulus, tensile and compressive strength remain important issues that are being currently pursued in our research laboratory. Further, generalization of the dispersion mechanism to other classes of polymers remains an outstanding issue for which general principles continue to be sought.

Acknowledgment. We thank Carbon Nanotechnologies, Inc., for the SWNTs and help with electrical conductivity measurements. Air Force Research Laboratory generously donated time on X27C at the NSLS at Brookhaven National Laboratory. We thank Xinfeng Shi for help with SEM and Dr. Carlos Avila Orta and Dr. Igor Sics for help at the NSLS at Brookhaven National Laboratory. Support of the Texas Institute for Intelligent Bio-Nano Materials and Structures for Aerospace Vehicles, funded by NASA Cooperative Agreement NCC-1-02038, is gratefully acknowledged. C.A.M. thanks NASA for partial funding through the Graduate Student Researchers Program.

References and Notes

(1) Ajayan, P. M.; Charlier, J.-C.; Rinzler, A. G. *Proc. Natl. Acad. Sci.* **1999**, *96*, 14199−14200. Saito, R.; Dresselhaus, G.; Dresselhaus, M. S. *Physical Properties of Carbon Nanotubes;* Imperial College Press: London, 1998.
(2) Mitchell, C. A.; Bahr, J. L.; Arepalli, S.; Tour, J. M.; Krishnamoorti, R. *Macromolecules* **2002**, *35*, 8825−8850.
(3) Putz, K. W.; Mitchell, C. A.; Krishnamoorti, R.; Green, P. F. *J. Polym. Sci., Part B: Polym. Phys.* **2004**, *42*, 2286−2293.
(4) Gong, X. Y.; Liu, J.; Baskaran, S.; Voise, R. D.; Young, J. S. *Chem. Mater.* **2000**, *12*, 1049−1052.
(5) Chatterjee, T.; Yurekli, K.; Hadjiev, V.; Krishnamoorti, R. *Adv. Funct. Mater.* **2005**, *15*, 1832−1838.
(6) Ausman, K. D.; Piner, R.; Lourie, O.; Ruoff, R. S.; Korobov, M. *J. Phys. Chem. B* **2000**, *104*, 8911−8915.
(7) Moore, V. C.; Strano, M. S.; Haroz, E.; Hauge, R. T.; Smalley, R. E. *Nano Lett.* **2003**, *3*, 1379−1382.
(8) Yurekli, K.; Mitchell, C. A.; Krishnamoorti, R. *J. Am. Chem. Soc.* **2004**, *126*, 9902−9903.
(9) Zhang, X.; Liu, T.; Sreekumar, T. V.; Kumar, S.; Moore, V. C.; Hauge, R. T.; Smalley, R. E. *Nano Lett.* **2003**, *3*, 1285−1288.
(10) Basiuk, E. V.; Basiuk, V. A.; Banuelos, J.-G.; Saniger-Bless, J.-M.; Pokrovskiy, V. A.; Gromovoy, T. Y.; Mischanchuk, A. V.; Mischanchuk, B. G. *J. Phys. Chem. B* **2002**, *106*, 1588−1597.
(11) Kong, J.; Dai, H. *J. Phys. Chem. B* **2001**, *105*, 2890−2893.
(12) Chattopadhyay, D.; Galeska, I.; Papadimitrakopoulos, F. *J. Am. Chem. Soc.* **2003**, *125*, 3370−3375.
(13) Chattopadhyay, D.; Lastella, S.; Kim, S.; Papadimitrakopoulos, F. *J. Am. Chem. Soc.* **2002**, *124*, 728−729.
(14) Hamon, M. A.; Chen, J.; Hu, H.; Chen, Y.; Itkis, M. E.; Rao, A. M.; Eklund, P. C.; Haddon, R. C. *Adv. Mater.* **1999**, *11* 834−840. Kahn, M. G. C.; Banerjee, S.; Wong, S. S. *Nano Lett.* **2002**, *2*, 1215−1218.
(15) Matarredona, O.; Rhoads, H.; Li, Z.; Harwell, J. H.; Balzano, L.; Resasco, D. E. *J. Phys. Chem. B* **2003**, *107*, 13357−13367.
(16) Nikolaev, P.; Bronikowski, M. J.; Bradley, R. K.; Rohmund, F.; Colbert, D. T.; Smith, K. A.; Smalley, R. E. *Chem. Phys. Lett.* **1999**, *313*, 91−97.
(17) Chen, J.; Hamon, M. A.; Hu, H.; Chen, Y.; Rao, A.; Eklund, P. C.; Haddon, R. C. *Science* **1998**, *282*, 95−98.
(18) Zhou, W.; Islam, M. F.; Wang, H.; Ho, D. L.; Yodh, A. G.; Winey, K. I.; Fischer, J. E. *Chem. Phys. Lett.* **2004**, *384*, 185−189.
(19) Hanley, I. J. M.; Muzny, C. D.; Ho, D. L.; Glinku, C. J. *Langmuir* **2003**, *19*, 5575.
(20) Bafna, A.; Beaucage, G.; Mirabella, F. *Polymer* **2003**, *44*, 1103−1115.
(21) Krishnamoorti, R.; Giannelis, E. P. *Macromolecules* **1997**, *30*, 4097−4102.
(22) Schaefer, D. W.; Zhao, J.; Brown, J.; Anderson, D. P.; Tomlin, D. W. *Chem. Phys. Lett.* **2003**, *375*, 369−375.
(23) de Gennes, P. G. *Scaling Concepts in Polymer Physics;* Cornell University Press: Ithaca, NY, 1979.
(24) Mitchell, C. A.; Krishnamoorti, R. *J. Polym. Sci., Part B: Polym. Phys.* **2002**, *40*, 1434−1443. Liu, C.; Zhang, J.; He, J.; Hu, G. *Polymer* **2003**, *44*, 7529−7532. Potschke, P.; Fornes, T. D.; Paul, D. R. *Polymer* **2002**, *43*, 3247−3255.
(25) Goel, V.; Chatterjee, T.; Bombalski, L.; Yurekli, K.; Matyjaszewski, K.; Krishnamoorti, R. *J. Polym. Sci., Part B: Polym. Phys.* **2006**, *44*, 2014−2023.
(26) Bonn, D.; Tanase, S.; Abou, B.; Tanaka, H.; Meunier, J. *Phys. Rev. Lett.* **2002**, *89*, 015701. Sollich, P.; Lequeux, F.; Hebraud, P.; Cates, M. E. *Phys. Rev. Lett.* **1997**, *78*, 2020−2023.
(27) Trappe, V.; Weitz, D. A. *Phys. Rev. Lett.* **2000**, *85*, 449−452.
(28) Ren, J.; Silva, A. S.; Krishnamoorti, R. *Macromolecules* **2000**, *33* 3739−3746. Ren, J. X.; Casanueva, B. F.; Mitchell, C. A.; Krishnamoorti, R. *Macromolecules* **2003**, *36*, 4188−4194.

(29) Yurekli, K.; Krishnamoorti, R.; Tse, M. F.; Mcelrath, K. O.; Tsou, A. H.; Wang, H.-C. *J. Polym. Sci., Part B: Polym. Phys.* **2001**, *39*, 256−275.
(30) Enikolopyan, N. S.; Fridman, M. L.; Stalnova, I. O.; Popov, V. L. *Adv. Polym. Sci.* **1990**, *96*, 1−67.
(31) Krishnamoorti, R.; Yurekli, K. *Curr. Opin. Colloid Interface Sci.* **2001**, *6*, 464−470.
(32) Garboczi, E. J.; Snyder, K. A.; Douglas, J. F.; Thorpe, M. F. *Phys. Rev. E* **1995**, *52*, 819−828.
(33) Vigolo, B.; Coulon, C.; Maugey, M.; Zakri, C.; Poulin, P. *Science* **2005**, *309*, 920−923.
(34) Youngs, I. J. *J. Phys. D: Appl. Phys.* **2002**, *35*, 3127−3137. Youngs, I. J. Electrical percolation and the design of functional electromagnetic materials. Ph.D., University College, London, 2001.
(35) Biercuk, M. J.; Liaguno, M. C.; Radosavljevic, M.; Hyun, J. K.; Johnson, A. T.; Fischer, J. E. *Appl. Phys. Lett.* **2002**, *80*, 2767−2769.
(36) O'Connell, M. J.; Bachilo, S. M.; Huffman, C. B.; Moore, V. C.; Strano, M. S.; Haroz, E. H.; Rialon, K. L.; Boul, P. J.; Noon, W. H.; Kittrell, C.; Ma, J.; Hauge, R. H.; Weisman, R. B.; Smalley, R. E. *Science* **2002**, *279*, 593−596.
(37) Kuo, S. W.; Huang, C. F.; Chang, F. C. *J. Polym. Sci., Part B: Polym. Phys.* **2001**, *39*, 1348−1359.
(38) Watanabe, T.; He, Y.; Asakawa, N.; Yoshie, N.; Inoue, Y. *Polym. Int.* **2001**, *50*, 463−468.

MA0616054